Surface-Plasmon Resonances in Single Metallic Nanoparticles

T. Klar, M. Perner, S. Grosse, G. von Plessen, W. Spirkl, and J. Feldmann
Lehrstuhl für Photonik und Optoelektronik, Sektion Physik, Ludwig-Maximilians-Universität, Amalienstraße 54, D-80799 München, Germany
(Received 4 February 1998)

Using a near-field optical antenna effect, we measure the homogeneous line shape of the surface-plasmon resonance in single gold nanoparticles. The surface-plasmon dephasing times extracted from the near-field spectra of the individual particles vary around 8 fs. This mean value agrees with calculations based on Mie theory, which neglect surface effects. Deviations of individual particles from this value are interpreted as being due to variations in the local nanoenvironment. We also observe double-peaked line shapes caused by electromagnetic coupling between close-lying particles. [S0031-9007(98)06063-3]

PACS numbers: 71.45.Gm, 07.79.Fc, 78.66.Bz

In metal nanoparticles, collective electron oscillations known as surface plasmons (SP's) can be excited by light. These elementary electronic excitations have been the subject of extensive research, both fundamental and with a view to applications [1]. In particles consisting of alkali, noble, and various other metals the SP's show themselves as pronounced optical resonances in the visible or UV parts of the spectrum. The resonance frequency of the oscillation, i.e., the SP energy, is essentially determined by the dielectric properties of the metal and the surrounding medium, and by the particle size and shape. The collective charge oscillation causes a large resonant enhancement of the local field inside and near the particle. This field enhancement is used in surface-enhanced Raman scattering (SERS) [2] and is currently discussed for potential applications in nonlinear optical devices [3], in optical tweezers [4], and generally for the manipulation of the local photonic density of states.

The properties of the SP are crucially influenced by its dephasing time $T_2 = 2\hbar/\Gamma_{\text{hom}}$, Γ_{hom} being the homogeneous linewidth of the SP resonance. For instance, the relation between the dephasing time and the local-field enhancement factor $|f|$ is given by $|f| \propto T_2$. This relation is particularly important for nonlinear optical effects: both the effective third-order susceptibility of metal particles [5] and the effective SERS cross section [6] are proportional to T_2^4. Microscopically, the SP dephasing time is controlled by coupling of the SP's to the electron-hole pair continuum [1], and by radiation damping, i.e., the decay of SP's into photons [5], which is important in large particles above a radius of ca. 10 nm. The first dephasing mechanism is strongly influenced by bulk electron scattering processes [7]; in addition, electron-surface scattering is believed to contribute for small particles sizes below $r = 10$ nm, or for high surface state densities, where chemical interface damping is important [1].

Despite the central importance of T_2, or Γ_{hom} for understanding the SP decay and for the local-field enhancement, it has been so far inaccessible to measurement due to the inhomogeneous broadening of the SP line. This inhomogeneous broadening can be caused by variations in the size, shape, surface structure, and dielectric environment of the individual particles within the cluster ensemble. Nonlinear optical techniques for measuring homogeneous linewidths fail in the present case: For instance, spectral hole burning requires that Γ_{hom} is much smaller than the total linewidth, a condition that generally is not fulfilled for metal particles, where $\Gamma_{\text{hom}} \sim \Gamma_{\text{total}}$. Using transient four-wave mixing to measure T_2 appears extremely difficult since SP dephasing times are believed to be on the order of 10 fs [8] and are thus too short to be reliably resolved with available laser pulses. In contrast, it appears promising to circumvent inhomogeneous broadening by selecting single particles *spatially* using the subwavelength resolution of near-field microscopy. This approach is encouraged by recent photon scanning tunneling microscopy (PSTM) experiments which have demonstrated light scattering from individual metal particles at selected wavelengths [9].

In this Letter we use a near-field optical antenna effect to measure the SP line shapes of single gold nanoparticles. We extract homogeneous linewidths, i.e., dephasing times for various spatially isolated particles. We find a typical dephasing time of 8 fs. The deviations of individual nanoparticles from this value are interpreted by assuming particle-to-particle variations in the local nanoenvironment. We also observe double-peaked line shapes which are explained by electromagnetic coupling between closely lying particles. Calculations based on Mie theory support our conclusions.

Figure 1 shows the experimental setup. A tunable cw laser illuminates the sample via the tapered Al coated fiber tip of a scanning near-field optical microscope (SNOM). The fiber tip has an aperture diameter of about 80 nm. The sample is a composite film of 200 nm thickness containing gold spheres with a radius of typically $r = 20$ nm embedded in a dielectric sol-gel TiO_2 matrix [10] with a refractive index of 2.19. The volume fill factor

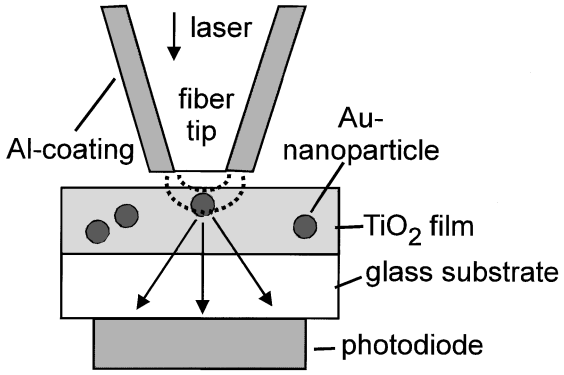

FIG. 1. Schematic setup: Laser light is coupled into the Al coated fiber tip which is kept 7 nm above the composite TiO_2 film. The dotted lines indicate the fiber's near-field lines; the arrows indicate the scattered radiation that is detected by the photodetector.

of the particles in the matrix is 3%. The upper part of Fig. 2 shows a far-field extinction spectrum of the sample, exhibiting an inhomogeneously broadened SP resonance at 1.96 eV and the onset of interband absorption at 2.38 eV. In the SNOM setup, the radiation transmitted through the composite film is detected by a Si photodetector fixed at the rear of a 1 mm thick glass substrate supporting the film. The distance between the tip aperture and the sample is kept at 7 nm by shear force control [11].

SNOM images taken at five different spectral positions are shown in Figs. 2(a)–2(e). Plotted is the transmitted light intensity scanned across a surface area of 750×750 nm^2. Figure 2(c), taken at a photon energy of 2.00 eV close to the peak of the far-field SP resonance, shows enhanced transmission at the spatial position of a nanoparticle in the center of the scan area. Figures 2(a) and 2(e) show that this transmission vanishes off resonance. A similar resonant enhancement is also observed at the spatial positions of other particles, reaching enhancement factors of up to 2.5 with respect to the background intensity. The enhancement effect is explained as follows: When there is a particle in the near field of the fiber tip aperture, its SP resonance is excited by the evanescent light modes from the tip and radiates propagating modes observable in the far field. In this sense, the particle acts as an "antenna" for the near field of the SNOM tip.

The high spatial resolution of the SNOM permits us to take transmission spectra of individual nanoparticles. Figure 3(a) shows the spectrally resolved transmission measured with the fiber tip fixed above a particular particle (denoted by #1 in the following). We plot here the relative transmission τ, i.e., the ratio of the transmitted intensity with and without a particle in the near field of the SNOM tip; $\tau > 1$ thus indicates a transmission enhancement. Figure 3(a) shows a peak at the spectral position of the far-field SP band (dashed line), with a linewidth that is markedly narrower. To evaluate the near-field spectrum, we note that the intensity of the field reradiated by the particle can be described by a near-field scattering efficiency that is resonantly enhanced by the SP [6]. The spectral line shape of the transmitted radiation thus directly reflects that of the SP, which means that the experiment presented here *gives access to the homogeneous linewidth and peak position of the surface plasmon in individual nanoparticles.* For example, this yields for particle #1 $\Gamma_{\mathrm{hom}} = 180$ meV [full width at half maximum (FWHM)] and $E_{\mathrm{peak}} = 1.95$ eV, respectively. In the time domain, $\Gamma_{\mathrm{hom}} = 180$ meV corresponds to a SP dephasing time of $T_2 = 7$ fs.

For a comparison of the experimental spectrum with theory, we consider the near-field scattering efficiency [6] Q_{NF}. In our case the electric dipole radiation (Mie theory expansion coefficient a_1 [1]) is dominant, rendering Q_{NF} nearly proportional to the far-field scattering efficiency,

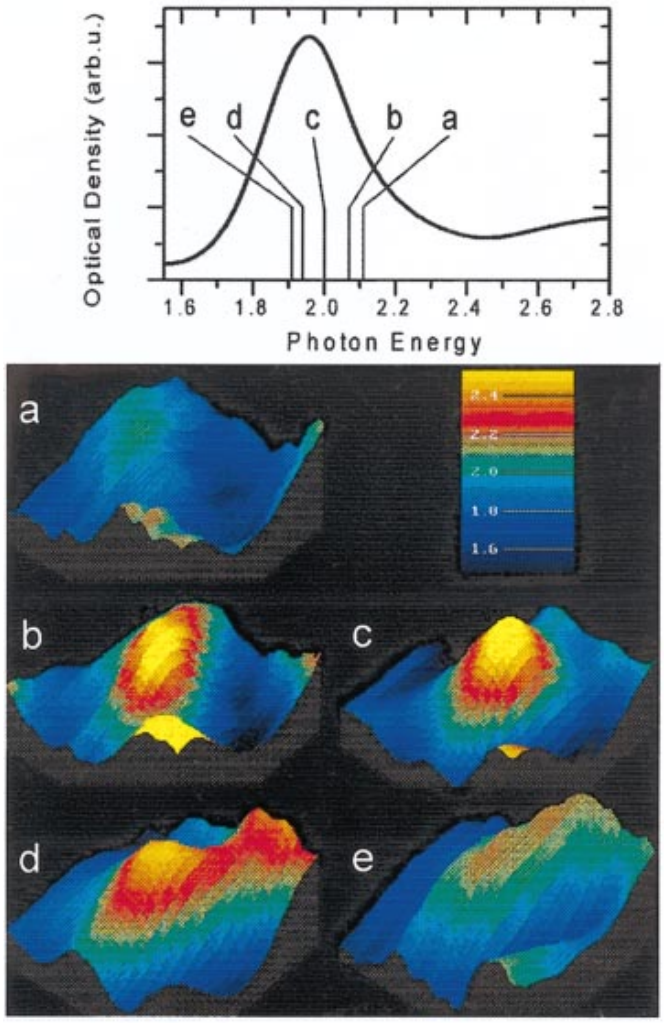

FIG. 2(color). Transmitted light intensity scanned across a surface area of 750×750 nm^2 (color scale in nW). Photon energies are (a) 2.11 eV, (b) 2.07 eV, (c) 2.00 eV, (d) 1.94 eV, and (e) 1.91 eV. Upper panel: Far-field extinction spectrum of the sample, with spectral positions of the SNOM images.

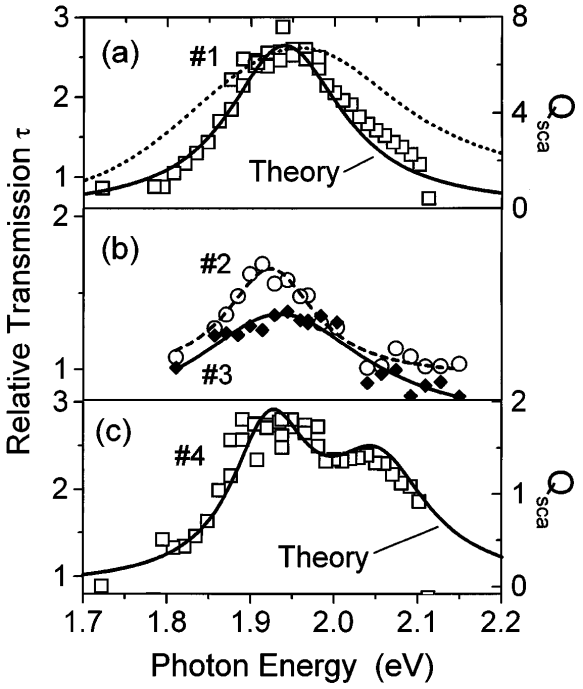

FIG. 3. Near-field transmission spectra of individual nanoparticles: (a) Particle #1 (squares); solid line: calculated Mie scattering efficiency Q_{sca}; dotted line: far-field optical density of the composite film in arbitrary units. (b) Particles #2 (circles) and #3 (diamonds); dashed and solid lines: Lorentzian fits to the data. (c) Object #4; solid line: theory.

Q_{sca}: $Q_{NF} \propto |a_1|^2 \propto Q_{sca}$. Therefore we calculate Q_{sca} for a direct comparison with the experimental data. The calculations are based on Mie theory [1], thus allowing for coupling of the SP to the electron-hole pair continuum and for radiation damping; electron-surface scattering processes are neglected. The calculations contain no adjustable parameters; bulk dielectric data from [12] are used, the spherical particle shape and the radius $r = 20$ nm are derived from transmission electron microscopy measurements, and the refractive index of the matrix has been determined by far-field transmission measurements on a sample containing no particles. Figure 3(a) shows that very good agreement with the experimental data is obtained for this particle.

We note, however, that the experimental spectra vary from particle to particle. For example, Fig. 3(b) shows the line shapes of two objects labeled #2 and #3 with linewidths of 130 and 250 meV, respectively. To analyze the variations in the particle spectra, we show in Fig. 4 the relation between the linewidth (FWHM) and the peak energy of spatially isolated particles; both quantities were determined by Lorentzian line fits to the data. Also shown is the relation expected from Mie theory for spheres of different sizes; the gradual increase in the linewidth with growing particle size is caused by a concomitant increase in radiation damping. For the particles investigated here, the measured peak energies are found to vary between 1.92 and 1.98 eV, probably due to variations in the particle size. The SP linewidths lie between 120 and 250 meV and thus below the far-field ensemble linewidth of $\Gamma_{total} = 300$ meV. For the majority of particles, the measured linewidths are relatively close to the results of the calculation. Larger deviations, like that of particle #3, might be interpreted by assuming particle-to-particle variations in the local nanoenvironment. Such variations could be caused by small fluctuations of the chemical composition of the nonperfectly compactified TiO_2 sol-gel matrix in our sample, which can lead to a higher local density of surface states at the metal/dielectric interface and hence to a larger chemical interface damping. The origin of the deviations from the theory requires further investigation; we restrict ourselves here to determining a representative value of Γ_{hom} by averaging over the 11 individual particles in Fig. 4. We obtain $\Gamma_{hom} = 160$ meV, which in the time domain corresponds to a SP dephasing time of $T_2 = 8$ fs. We use this information to calculate the local-field enhancement at the particle surface; we obtain an orientationally averaged local-field enhancement factor of $|f| = 12$ with respect to the external field. Such information on T_2 drawn from SNOM measurements can be used in a systematic way to maximize the local-field enhancement for applications like SERS, optical tweezers, nonlinear optical devices, and spatially resolved photochemical conversion [13]. Furthermore, information on T_2 should help to analyze fundamental electronic decay processes in the metal nanoparticles [1,7].

Besides the line shapes of isolated particles, also other types of spectra are found. Object #4 in Fig. 3(c) exhibits a double-peak structure, where the higher-energy peak lies at 2.05 eV, well above those of all isolated particles studied here. We suggest that this structure is caused by a line splitting due to electromagnetic coupling of two close-lying particles [14]. In order to support this assumption, we have calculated the line shape of aggregates of two identical spheres of radius r separated from each other by a distance d and electromagnetically coupled to each other. Each sphere is considered as a dipole with polarizability

$$\alpha = 6\pi k^{-3} i a_1 , \qquad (1)$$

where k is the wave vector in the matrix and i is the imaginary unit. As shown in Fig. 3(c), the orientationally averaged far-field scattering efficiency [15] of an aggregate with $r = 10$ nm and $d = 6$ nm closely matches the observed double peak. We note that although $r = 10$ nm is quite far from the peak of the particle-size distribution, it is well within the possible size range.

The data in Figs. 3(a)–3(c) and 4 indicate a large variety in the nanoparticle spectra, which lies "hidden" below the inhomogeneously broadened SP line shape of the far-field ensemble spectrum. In this sense, near-field spectroscopy on individual metal nanoparticles makes

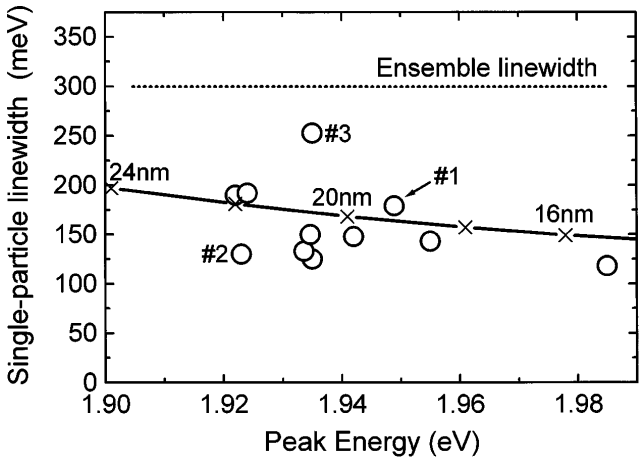

FIG. 4. Linewidth vs peak energy determined from the near-field spectra of individual nanoparticles (circles). Solid line: theoretical results for gold spheres of different radii. Dashed line: ensemble linewidth (300 meV) as determined from the far-field extinction spectrum in Fig. 2.

possible the observation of local dielectric effects that would remain unnoticed otherwise, like, e.g., the mode splitting in Fig. 3(c) indicating the coupling of two particles. In the future, this could be used to extend the capabilities of SP-based chemical and biological sensors [16,17], giving them all the advantages of high spatial resolution beyond the diffraction limit. For instance, marking of cell structures with gold nanoparticles, which is routinely employed in electron microscopy, could be used in combination with near-field spectroscopy to produce *dielectric images* of those structures with nanometer spatial resolution.

In summary, we have performed SNOM spectroscopy on individual gold nanoparticles. We have measured for the first time the homogeneous line shape of the surface-plasmon resonance in a metallic system. The homogeneous SP linewidth is substantially smaller than the ensemble linewidth, and varies around a value of 160 meV; this corresponds to a SP dephasing time of 8 fs, and agrees with the results of a Mie-theory calculation. Deviations of individual particles from this value can be explained by assuming variations in the local nanoenvironment of the particles. Besides the singe-mode resonances, we also observe more complex line shapes caused by electromagnetic coupling between close-lying particles. SNOM spectroscopy on individual metal nanoparticles holds great promise for optically probing and manipulating the local nanoenvironment of the particles.

We thank the *Institut für Neue Materialien* in Saarbrücken for providing the nanoparticle samples, K. Karrai and C. Obermüller for generous support in setting up the SNOM, U. Lemmer, F. R. Aussenegg, and L. Novotny for fruitful discussions, and W. Stadler for excellent technical support. Financial support by the Deutsche Forschungsgemeinschaft and by the European Union (within the network *Ultrafast Quantum Optoelectronics*) is gratefully acknowledged.

[1] U. Kreibig and M. Vollmer, *Optical Properties of Metal Clusters* (Springer, Berlin, 1995).
[2] S. Nie and S. R. Emory, Science **275**, 1102 (1997).
[3] J. W. Haus, N. Kalyaniwalla, R. Inguva, and C. M. Bowden, J. Appl. Phys. **65**, 1420 (1989).
[4] L. Novotny, R. X. Bian, and X. S. Xie, Phys. Rev. Lett. **79**, 645 (1997).
[5] E. J. Heilweil and R. M. Hochstrasser, J. Chem. Phys. **82**, 4762 (1985).
[6] B. J. Messinger, K. U. von Raben, R. K. Chang, and P. W. Barber, Phys. Rev. B **24**, 649 (1981).
[7] M. Perner, P. Bost, U. Lemmer, G. v. Plessen, and J. Feldmann, Phys. Rev. Lett. **78**, 2192 (1997).
[8] K. Puech, F. Z. Henari, W. J. Blau, D. Duff, and G. Schmid, Chem. Phys. Lett. **247**, 13 (1995).
[9] J. R. Krenn, W. Gotschy, D. Somitsch, A. Leitner, and F. R. Aussenegg, Appl. Phys. A **61**, 541 (1995).
[10] M. Mennig, U. Becker, M. Schmitt, and H. Schmidt, in *Proceedings of the 8th International Conference on Modern Materials & Technologies (CIMTEC), Florence, 1994, Adv. Materials in Optics, Electro-Optics and Communication Technologies*, edited by P. Vincenzini (Techna, Florence, 1995), pp. 39–46.
[11] K. Karrai and R. D. Grober, Appl. Phys. Lett. **66**, 1842 (1995).
[12] P. B. Johnson and R. W. Christy, Phys. Rev. B **6**, 4370 (1972).
[13] M. Moskovits, Rev. Mod. Phys. **57**, 783 (1985).
[14] A. Berger, K.-J. Berg, and H. Hofmeister, Z. Phys. D **20**, 309 (1991).
[15] B. T. Draine and P. J. Flatau, J. Opt. Soc. Am. A **11**, 1491 (1994).
[16] T. Brandt, W. Hoheisel, A. Iline, F. Stietz, and F. Träger, Appl. Phys. B **65**, 793 (1997).
[17] R. Elghanian, J. J. Storhoff, R. C. Mucic, R. L. Letsinger, and C. A. Mirkin, Science **277**, 1078 (1997).